

Detection of localized ferromagnetic resonance in a continuous thin film via magnetic resonance force microscopy

E. Nazaretski,¹ D. V. Pelekhov,² I. Martin,¹ M. Zalalutdinov,³ D. Ponarin,⁴ A. Smirnov,⁴ P. C. Hammel,² and R. Movshovich¹

¹Los Alamos National Laboratory, Los Alamos, New Mexico 87545, USA

²Department of Physics, Ohio State University, Columbus, Ohio 43210, USA

³SFA Inc., Crofton, Maryland 21114, USA

⁴Department of Chemistry, North Carolina State University, Raleigh, North Carolina 27695, USA

(Received 15 August 2008; published 2 April 2009)

We present magnetic resonance force microscopy (MRFM) measurements of ferromagnetic resonance in a 50 nm thick permalloy film tilted with respect to the direction of the external magnetic field. At small probe-sample distances the MRFM spectrum breaks up into multiple modes, which we identify as local ferromagnetic resonances confined by the magnetic field of the MRFM tip. Micromagnetic simulations support this identification of the modes and show they are stabilized in the region where the dipolar tip field has a component antiparallel to the applied field.

DOI: [10.1103/PhysRevB.79.132401](https://doi.org/10.1103/PhysRevB.79.132401)

PACS number(s): 76.50.+g, 07.55.-w, 07.79.Pk, 75.70.-i

Magnetic resonance force microscopy (MRFM) (Ref. 1) provides a route to detection of magnetic resonance with excellent spin sensitivity and spatial resolution and has received considerable attention. Detection of electron-spin resonance,² nuclear magnetic resonance,³ and ferromagnetic resonance (FMR) (Refs. 4–7) with this approach has been reported. The high sensitivity of MRFM when combined with the imaging mechanism of magnetic resonance imaging (MRI) allows excellent spatial resolution in noninteracting spin systems.⁸ Studies of patterned films show that FMR can be detected in individual microstructures with high sensitivity.^{4–6,9} As a consequence of the strong interactions between spins in a ferromagnet the excitations are collective (magnetostatic) modes, so the assumptions on which MRI is based are invalidated. However recent work shows that MRFM is also a promising technique for spatially resolved FMR. Obukhov *et al.*¹⁰ at OSU demonstrated that the large field gradient of the micromagnetic probe enables ferromagnetic resonance imaging of the magnetostatic modes of a 2 μm diameter permalloy dot with ~ 250 nm resolution.

Here we argue that the micromagnetic probe *locally stabilizes magnetostatic modes* detected in FMR thus indicating the potential for scanned probe imaging of magnetic properties of extended ferromagnetic films. Due to the strong interaction between the spins the resonance modes are collective excitations of spins in the entire sample, and in the case of the microfabricated samples, the FMR modes are defined by the geometry of the sample.

We study the dependence of the mode resonance field on the orientation of the film relative to the external magnetic field and on the probe-sample separation. We find that localized FMR modes are spatially confined immediately below the MRFM probe magnet. This occurs because off the axis of the micromagnetic probe its dipolar field is negative and so reduces the magnitude of the total magnetic field stabilizing a confined mode. To understand the nature of these modes and their behavior, we performed micromagnetic simulations based on a finite element solution of the Landau-Lifshitz (LL) equation with damping. The simulations reveal that the degree of localization can be controlled not only by the

sample-probe separation, but that it is also very sensitive to the tilt angle between the film and the applied magnetic field. These results demonstrate confinement of the magnetostatic mode by the localized inhomogeneous field of the probe, a mechanism distinct from geometrical confinement such as was studied in Ref. 10.

The MRFM experiments were performed with the low-temperature dual magnetic force microscopy (MFM)/MRFM apparatus at Los Alamos National Laboratory. We used a commercially available silicon nitride cantilever (resonance frequency $f_c \approx 8.0$ kHz and spring constant $k \sim 10$ mN/m). The micromagnetic probe tip is a 2.4 μm diameter spherical $\text{Nd}_2\text{Fe}_{14}\text{B}$ particle. Its silicon nitride tip was removed by focused ion milling, and the magnetic sphere was manually glued to the cantilever in the presence of an aligning magnetic field of a few kilo-Oersteds. The saturation magnetization of $\text{Nd}_2\text{Fe}_{14}\text{B}$ powder was determined to be $4\pi M_s \approx 13.2$ kG at 10 K using superconducting quantum interference device (SQUID) magnetometry. The spatial field profile produced by the probe magnet has been carefully characterized.¹¹ For a detailed description of the MRFM apparatus we refer the reader to Ref. 12.

The 50 nm thick permalloy film was deposited on a 100 μm thick silicon wafer on top of a 20 nm thick Ti adhesion layer and capped with a protective 20 nm Ti layer. An approximately 1.9×1.9 mm² sample was glued to the strip line microwave resonator. The temperature of the sample was stabilized at $T = 11$ K (temperature stability was better than 5 mK) and the frequency of the microwave field was set to $f_{\text{RF}} = 9.75$ GHz. Figure 1 shows a schematic diagram of the experiment.

The in-phase component of the lock-in detected MRFM signal is shown in Fig. 2 as a function of the probe-sample separation for three values of the tilt angle Θ between the normal to the film plane and the direction of \mathbf{H}_{ext} (as shown in Fig. 1). The sample tilt angles were determined by measuring the deflection of a laser beam reflected off the film surface at room temperature and found to be 1.0° , 3.4° , and 5.4° . While the absolute uncertainty of the sample tilt at low temperatures is $\approx \pm 1.0^\circ$, mainly due to thermal contraction

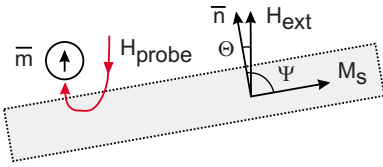


FIG. 1. (Color online) Schematic of the experiment. The sample is tilted and placed in the uniform external magnetic field H_{ext} . Here \hat{n} is the normal to the sample surface, Θ is the sample tilt angle with respect to H_{ext} , and Ψ is the tilt angle of the equilibrium magnetization M_s . The MRFM probe field is aligned with the direction of H_{ext} and its dipolar field reduces the magnitude of H_{ext} in the region off to the side of the magnetic tip \mathbf{m} .

of the glue used to hold the sample in place, the relative uncertainty of the tilt angles at low temperature is better than 0.1° . These tilt angles were confirmed by the measured values of the resonance field H_{ext} at large probe-sample separations (discussed further below).

All spectra shown in Fig. 2 exhibit very similar evolution as a function of probe-sample separation. A single fundamental resonance mode is observed at distances greater than a few micrometers. The resonance field of this mode changes as the probe approaches the sample surface [Fig. 2(a)]. At

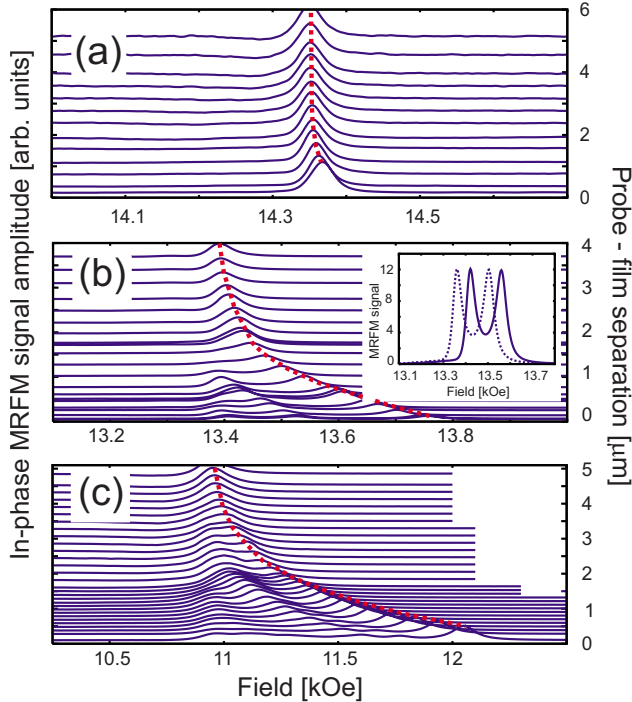


FIG. 2. (Color online) The in-phase component of the MRFM signal. Each spectrum is plotted with an offset proportional to the probe-sample separation. This separation can be read off of the right-hand vertical axis far from resonance. Spectra were recorded at three different angles Θ : (a) 1.0° , (b) 3.4° , and (c) 5.4° at $T = 11$ K and $f_{\text{RF}} = 9.75$ GHz. Note the different horizontal axis scales for each panel. Red dotted line traces the evolution of the fundamental resonance mode. Spectra were scaled for clarity of presentation. Inset in (b) shows the shift of the entire resonance structure with the change of the microwave frequency from 9.75 to 9.65 GHz at a probe-film separation of ~ 760 nm.

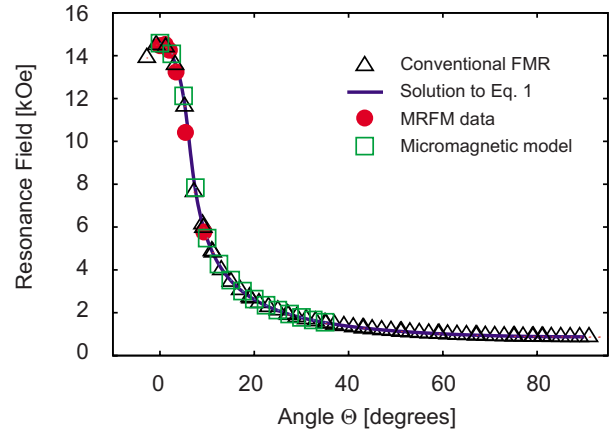


FIG. 3. (Color online) Angular dependence of the resonance field for the uniform H_{ext} . The four data sets—conventional FMR data (Δ), solution to Eq. (1) (solid line), MRFM data at large probe-sample separation (\bullet), and the results of the micromagnetic modeling (\square)—are in good agreement. The numerical solution and the micromagnetic modeling were done using the same simulation parameters $4\pi M_s = 11.3$ kG, $f_{\text{RF}} = 9.5$ GHz, and $\gamma = 2.89 \pm 0.05$ GHz/kOe. MRFM data were acquired at $f_{\text{RF}} = 9.75$ GHz.

larger values of Θ [Figs. 2(b) and 2(c)] splitting of the fundamental mode is observed at small separations. The magnitude of the splitting increases with increasing Θ [Fig. 2(c)].

In order to better understand the evolution of the MRFM signal, we performed FMR studies as a function of Θ in a conventional FMR spectrometer. In Fig. 3 we show the angular dependence of the resonance field for the permalloy sample. Conventional FMR experiments were performed at NCSU. Data were obtained in a uniform applied field H_{ext} and are equivalent to the MRFM resonance spectra acquired at large values of the probe-sample separation. In fact, the MRFM and conventional FMR sets of data exhibit excellent agreement as shown in Fig. 3. The value of the ferromagnetic resonance field in a continuous film for a given Θ is determined by the dispersion relation¹³

$$\left(\frac{\omega}{\gamma}\right)^2 = [H_{\text{ext}} \cos(\Theta - \Psi) - 4\pi M_s \cos(2\Psi)] \times [H_{\text{ext}} \cos(\Theta - \Psi) - 4\pi M_s \cos^2(\Psi)], \quad (1)$$

$$H_{\text{ext}} \sin(\Theta - \Psi) + 2\pi M_s \sin(2\Theta) = 0. \quad (2)$$

Here $\omega = 2\pi f_{\text{RF}}$ is the RF, γ is the gyromagnetic ratio, $4\pi M_s$ is the saturation magnetization, and Ψ is the tilt angle of the equilibrium magnetization as shown in Fig. 1. We neglect the anisotropy contribution because it is typically small (around few Gauss) in uniform permalloy films.^{14,15} Equations (1) and (2) cannot be solved analytically, so we solved them numerically; the results are shown in Fig. 3 by the solid line. We used the conventional FMR data set to verify the values of $4\pi M_s = 11.3$ kG and $\gamma = 2.89 \pm 0.05$ GHz/kOe. With conventional FMR we never observed any multiple resonance structures reminiscent of those appearing in Fig. 2.

The origin of the isolated resonance modes seen in the MRFM studies can be understood in the following way. Con-

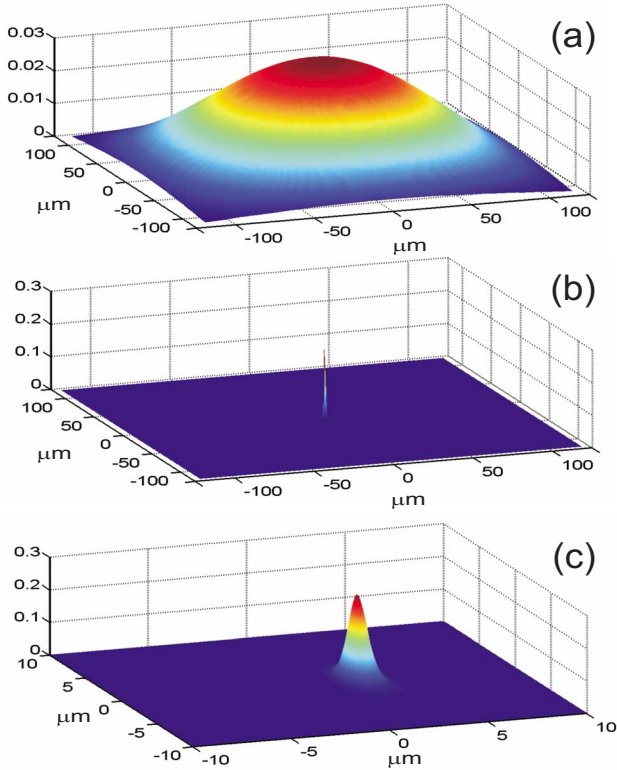


FIG. 4. (Color online) Numerically calculated spatial profile of the excited transverse magnetization of the fundamental FMR mode in a $250 \times 250 \mu\text{m}^2$ permalloy film. The thickness of the film is 50 nm and it is tilted at an angle Θ with respect to the direction of the applied magnetic field. The probe magnet is a $2.4 \mu\text{m}$ diameter sphere placed at a distance d over the center of the film, $(0, 0, d)$ (a) $\Theta=0^\circ$, no probe magnet (b) $\Theta=5.99^\circ$, $d=1.0 \mu\text{m}$; localized FMR mode at the location of the probe can be seen. (c) Zoom-in onto the localized mode. Due to the sample tilt, the peak mode is localized to the side of the probe. All modes were calculated for the value of H_{ext} corresponding to $f_{\text{RF}}=9.75$ GHz.

ventional FMR theory assumes a uniform magnetic field throughout the sample.¹⁶ The LL analysis shows that the presence of a position dependent inhomogeneous magnetic field of the probe may result in a formation of localized FMR modes confined to the region where the field inhomogeneity exceeds the value of $\Delta H_{\text{max}} \approx 2\pi M_s(L/a)$ (where L is the thickness of the film and a is the radius of the localization).¹⁰ The MRFM probe produces an approximately dipolar field in the plane of the sample. In the simplest geometry \mathbf{H}_{ext} and the tip's magnetic moment \mathbf{m} are parallel to each other. In this case the total magnetic field directly under the tip (uniform external field plus the dipolar field due to the tip) is higher than the external field, but off to the side it is lower than \mathbf{H}_{ext} (see Fig. 1). In these two loci the field at which resonance occurs is shifted to higher and lower fields, respectively, relative to resonance in the external field alone. While the modes shifted down in field may overlap with the bulk magnetostatic modes, the modes shifted up in field are well isolated so they can readily be used to perform local MRFM spectroscopy.

In order to quantify this picture we have conducted mi-

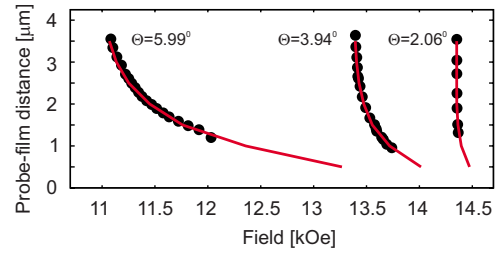


FIG. 5. (Color online) Comparison of the numerically calculated evolution of the fundamental FMR mode (solid line) with data points taken from Fig. 2 (filled circles). The micromagnetic modeling was performed for the tilt angles obtained from the resonance fields of the fundamental mode at large probe-sample separations. To obtain the agreement shown in Fig. 5 we had to increase the measured probe-sample separation by $\approx 1 \mu\text{m}$ (depending on the tilt angle). The origin of the offset is the short-range probe-sample interaction which causes the cantilever to snap to the film at probe-sample distances less than $1 \mu\text{m}$. The nature of the interaction has been discussed in Refs. 19 and 20 and the magnitude of the offset has been quantified in Ref. 11.

cro-magnetic simulations based on the LL equation with damping

$$\frac{\partial \mathbf{M}}{\partial t} = \gamma \mathbf{M} \times \mathbf{H}_{\text{tot}} - \frac{\lambda}{M_s^2} \mathbf{M} \times \mathbf{M} \times \mathbf{H}_{\text{tot}}, \quad (3)$$

where λ is the damping coefficient. The total magnetic field \mathbf{H}_{tot} experienced by the sample magnetization \mathbf{M} consists of the external, probe, dipolar, exchange, and anisotropy fields. The numerical solution of Eq. (3) for this field configuration provides the information about the spatial profile of the FMR modes excited in the sample and their corresponding resonance fields. The details of the numerical approach and its application to a variety of systems will be presented elsewhere.¹⁷

As numerical simulation of an infinite ferromagnetic film with an inhomogeneous external field profile is difficult we simulated a finite ferromagnetic thin film that was large compared to the phenomena of interest ($250 \times 250 \mu\text{m}^2$ square with thickness 50 nm). The magnetic parameters chosen for simulations were obtained from the conventional FMR experiment: $4\pi M_s = 11.3$ kG and $\gamma = 2.89$ GHz/kOe. For the damping we used $\lambda = 0.005 \text{ s}^{-1}$, a typical value for permalloy. Equation (3) was linearized on a variable density pixel grid with higher pixel density in the vicinity of the probe magnet. The rare-earth probe magnet was modeled as a $2.4 \mu\text{m}$ diameter uniformly magnetized sphere ($4\pi M_s = 13.2$ kG) placed at a height d measured from the surface of the film. The probe was positioned over the center of the film. Probe magnet parameters were experimentally determined in Refs. 7 and 11. The orientation of the probe magnetic moment \mathbf{m} is assumed to be aligned with the direction of \mathbf{H}_{ext} . The validity of the modeling approach was verified by comparing the modeling results for a tilted film (without MRFM tip) with the conventional FMR data (see Fig. 3). In the absence of the localized probe field, the fundamental (lowest frequency) resonance mode has a well-known bell-shaped spatial profile, as shown in Fig. 4(a), and spans the

entire sample. This result is in good agreement with earlier theoretical work.¹⁸ In the presence of the probe magnet, however, the mode changes its shape dramatically and is spatially confined to the region immediately beneath the probe magnet [see Fig. 4(b)]. A closer look at the mode localization [see Fig. 4(c)] reveals confinement on the order of a few μm^2 . This is the region of the sample where the dipolar field of the probe magnet opposes the externally applied field \mathbf{H}_{ext} . The asymmetry in the shape of the localized FMR mode with respect to the position of the probe magnet is due to the tilt of the sample, as illustrated in Fig. 1.

In Fig. 5 we compare the micromagnetic simulations of the evolution of the fundamental mode to the experimental points taken from the dotted line in Fig. 2. The values of the sample tilt angle Θ used in simulation were chosen to match the values of the resonance field \mathbf{H}_{ext} at large probe-sample separations. It can be seen that the value of \mathbf{H}_{ext} shifts toward higher values as the probe approaches the sample. This shift also increases with increasing tilt angle of the sample. This is consistent with the increase of the probe's negative field, which would require higher values of \mathbf{H}_{ext} to satisfy the spin-resonance condition at $f_{\text{RF}}=9.75$ GHz.

In conclusion, we have observed FMR modes stabilized in a confined region defined by the localized field of micromagnetic probe field. These are observed when the sample is tilted with respect to the orientation of the probe axis thus subjecting the sample to the negative dipolar field produced off the axis of the probe magnet. Our micromagnetic simulations accurately describe the experiments and find the modes to be confined to a region of order a micron across. Our experiments point to the possibility of spatially resolved FMR (e.g., imaging and characterization of defects and magnetic inhomogeneities) in continuous ferromagnetic films.

We thank T. Mewes for stimulating discussions and B. Houston and J. W. Baldwin for sample fabrication. The work performed at Los Alamos National Laboratory was supported by the U.S. Department of Energy, Center for Integrated Nanotechnologies. The work at OSU was supported by the U.S. Department of Energy through Grant No. DE-FG02-03ER46054. This work was also supported by the Office of Naval Research through the Institute for Nanoscience at Naval Research Laboratory. The work at NCSU was supported by NSF under Grant No. ECS-0420775.

-
- ¹J. A. Sidles, Appl. Phys. Lett. **58**, 2854 (1991).
²D. Rugar, C. S. Yannoni, and J. A. Sidles, Nature (London) **360**, 563 (1992).
³D. Rugar, O. Züger, S. Hoen, C. S. Yannoni, H. M. Vieth, and R. D. Kendrick, Science **264**, 1560 (1994).
⁴Z. Zhang, P. C. Hammel, and P. E. Wigen, Appl. Phys. Lett. **68**, 2005 (1996).
⁵G. de Loubens, V. V. Naletov, O. Klein, J. B. Youssef, F. Boust, and N. Vukadinovic, Phys. Rev. Lett. **98**, 127601 (2007).
⁶K. Wago, D. Botkin, C. S. Yannoni, and D. Rugar, Appl. Phys. Lett. **72**, 2757 (1998).
⁷E. Nazaretski, I. Martin, R. Movshovich, D. V. Pelekhov, P. C. Hammel, M. Zalalutdinov, J. W. Baldwin, B. Houston, and T. Mewes, Appl. Phys. Lett. **90**, 234105 (2007).
⁸H. J. Mamin, M. Poggio, C. L. Degen, and D. Rugar, Nat. Nanotechnol. **2**, 301 (2007).
⁹M. M. Midzor, P. E. Wigen, D. Pelekhov, W. Chen, P. C. Hammel, and M. L. Roukes, J. Appl. Phys. **87**, 6493 (2000).
¹⁰Yu. Obukhov, D. V. Pelekhov, J. Kim, P. Banerjee, I. Martin, E. Nazaretski, R. Movshovich, S. An, T. J. Gramila, S. Batra, and P. C. Hammel, Phys. Rev. Lett. **100**, 197601 (2008).
¹¹E. Nazaretski, E. A. Akhadov, I. Martin, D. V. Pelekhov, P. C. Hammel, and R. Movshovich, Appl. Phys. Lett. **92**, 214104 (2008).
¹²E. Nazaretski, T. Mewes, D. Pelekhov, P. C. Hammel, and R. Movshovich, AIP Conf. Proc. **850**, 1641 (2006).
¹³P. Wigen, Thin Solid Films **114**, 135 (1984).
¹⁴Z. Frait, Physica B & C **86-88**, 1241 (1977).
¹⁵E. Nazaretski, J. D. Thompson, M. Zalalutdinov, J. W. Baldwin, B. Houston, T. Mewes, D. V. Pelekhov, P. Wigen, P. C. Hammel, and R. Movshovich, J. Appl. Phys. **101**, 074905 (2007).
¹⁶S. V. Vonsovskii, *Ferromagnetic Resonance* (Pergamon, Oxford, 1966).
¹⁷D. V. Pelekhov, I. Martin, and P. C. Hammel (unpublished).
¹⁸G. N. Kakazei, P. E. Wigen, K. Yu. Guslenko, V. Novosad, A. N. Slavin, V. O. Golub, N. A. Lesnik, and Y. Otani, Appl. Phys. Lett. **85**, 443 (2004).
¹⁹M. Saint Jean, S. Hudlet, C. Guthmann, and J. Berger, J. Appl. Phys. **86**, 5245 (1999).
²⁰S. Hudlet, M. Saint Jean, C. Guthmann, and J. Berger, Eur. Phys. J. B **2**, 5 (1998).